Geomorphology 303 (2018) 456–466

Contents lists available at ScienceDirect

Geomorphology

journal homepage: www.elsevier.com/locate/geomorph

Modulation of the erosion rate of an uplifting landscape by long-term climate change: An experimental investigation

Bérangé Moussirou, Stéphane Bonnet *

Université de Toulouse, Géosciences Environnement Toulouse, UPS, CNRS UMR 5563, 14 avenue E Belin, 31400 Toulouse, France

ARTICLE INFO

Article history:
Received 24 August 2017
Received in revised form 3 December 2017
Accepted 3 December 2017
Available online 7 December 2017

Keywords:
Landscape evolution
Experimental modeling
Relief
Erosion
Climate

ABSTRACT

Whether or not climatic variations play a major role in setting the erosion rate of continental landscapes is a key factor in demonstrating the influence of climate on the tectonic evolution of mountain belts and understanding how clastic deposits preserved in sedimentary basins may record climatic variations. Here, we investigate how a change in precipitation influences the erosional dynamics of laboratory-scale landscapes that evolved under a combination of uplift and rainfall forcings. We consider here the impact of a decrease in the precipitation rate of finite duration on the erosive response of a landscape forced by a constant uplift and initially at a steady state (SS1). We performed several experiments with the same amplitude but different durations of precipitation decrease (*Tp*). We observe that the decrease in precipitation induces a phase of surface uplift of landscapes to a new steady state condition (SS2); however, the details of the uplift histories (timing, rate) differ between the experiments according to *Tp*. We also observe a decrease in the erosion rate induced by the precipitation change; however, the timing and amplitude of this decrease vary according to *Tp*, defining a delayed and damped erosion signal. Our data show that the landscape response to precipitation change is dictated by a critical water-to-rock ratio (ratio of precipitation over uplift) that likely corresponds to a geomorphic threshold. Our study suggests that variations in precipitation that occur at a geological time scale ($>10^6$ years) may have a weak impact on the erosion of landscapes and on the delivery of siliciclastic material to large rivers and sedimentary basins.

1. Introduction

Whether or not climatic variations, and in particular precipitation variations, play a major role in defining the long-term erosion rates ($>10^{5-6}$ years) of continental landscapes is a key factor in demonstrating the influence of climate on the tectonic evolution of mountain belts, as expected from analytical, numerical, and analog modeling approaches (e.g., Dahlen et al., 1984; Willett, 1999; Whipple and Meade, 2006). These models demonstrate that modifications in the erosion rate that would significantly affect the gravitational loading of the continental crust might change its state of stress and consequently its deformation. However, field evidence of these interactions has proved challenging to unambiguously demonstrate (Whipple, 2009), the question of climatic control on erosion efficiency at a geological time scale being among the most critical issues (Whipple, 2009). If we only consider precipitation, for example, its effect on long-term erosion is controversial because erosion rates inferred from cosmogenic or thermochronologic studies sometimes correlate with its mean annual value (e.g., Reiners et al., 2003; Thiede et al., 2004; Moon et al., 2011; Bookhagen and Strecker, 2012) but do not or only weakly correlate in other cases (e.g., Riebe et al., 2001; Burbank et al., 2003; von Blanckenburg, 2005; Carretier et al., 2013; Godard et al., 2014). Similarly, a link between precipitation and landscape metrics is rarely observed in nature (e.g., Champagnac et al., 2012) or is difficult to highlight (D'Arcy and Whittaker, 2014), whereas it is expected theoretically (e.g., Whipple et al., 1999). Our inability to distinctly understand the effect of precipitation on landscape and erosion may be related to many phenomena. Taking into account orographic effects, for example, modifies the expected relationship between landscape metrics, such as the steepness index and precipitation rate (D'Arcy and Whittaker, 2014). Actually, although theory indicates that high steady state reliefs develop under low erosional efficiency conditions (dry climate) (Whipple et al., 1999), in many cases topography and climate are coupled, and consequently precipitation increases because of orographic effects during the uplift of a high mountain. Orographic precipitation, however, is not at a maximum at the highest elevations but commonly between 1000 and 2000 m (e.g., Bookhagen and Burbank, 2006). In such a context, deconvolving the climatic and tectonic influences on erosion rates is difficult (D'Arcy and Whittaker, 2014; Deeken et al., 2011), a problem that was likely magnified by the development of glaciations during the Plio-Pleistocene, which enhanced erosion in mountains worldwide (Herman et al., 2013).

The question of landscape sensitivity to the time-scale of climatic variations is another major issue that needs to be considered in

* Corresponding author.
E-mail address: stephane.bonnet@get.omp.eu (S. Bonnet).

https://doi.org/10.1016/j.geomorph.2017.12.010
0169-555X/

understanding the impact of precipitation on landscapes and erosion. It has been proposed, for example, that the change in the periodicity of the global climate during the Plio-Pleistocene could explain the global increase in continental erosion deduced from the terrigenous sedimentation rate observed in oceans worldwide (e.g., Zhang et al., 2001). However, this latter observation is strongly disputed (see, for example, the synthesis of Willenbring and Jerolmack, 2016). Numerical models have shown that the response of a landscape to periodic changes in precipitation depends on the frequencies considered (Godard et al., 2013; Braun et al., 2015), with a specific periodicity that maximizes the erosional response (Godard et al., 2013); thus, if forced by an uplift, the erosion rate of such a landscape continuously oscillates around the uplift rate value. In contrast, for longer forcing periods, the landscape is always adjusted to the precipitation conditions and is in a steady state so its erosion rate is always equal to that of the uplift and remains constant in time (Godard et al., 2013; 'reactive landscapes' of Allen, 2008). This result is important because it indicates that depending on the forcing periodicity, erosion rates are related (or not) to precipitation, depending on the equilibrium state of the landscape (see also Bonnet and Crave, 2003). The landscape response to climatic variation and its related erosional signal are also potentially influenced by the presence of geomorphic thresholds that are sensitive to climate. It has been suggested for example that the location of channel heads is governed by a threshold for runoff erosion related to shear stress (Horton, 1945; Montgomery and Dietrich, 1992) and then, that the extent of the channel network (drainage density) could vary according to climate (Montgomery and Dietrich, 1992; Rinaldo et al., 1995; Tucker and Slingerland, 1997). Interestingly, numerical simulations show that the existence of such a threshold can drive a punctuated erosion in response to smoothly varying climate (Tucker and Slingerland, 1997).

We investigate here the landscape and erosive responses to climate change on laboratory experiments, following the work of Bonnet and Crave (2003). Such physical experiments offer a powerful means for understanding landscape evolution and testing hypotheses under controlled forcings (e.g., Hasbargen and Paola, 2000, 2003; Bonnet and Crave, 2003; Lague et al., 2003; Babault et al., 2005, 2007; Turowski et al., 2006; Bonnet, 2009; Reinhardt and Ellis, 2015; Singh et al., 2015; Sweeney et al., 2015). In the experiments here, the precipitation rate decreased after a first phase of precipitation and uplift and the attainment of a steady state between erosion and uplift (Lague et al., 2003; Bonnet and Crave, 2003), considering different durations of precipitation decrease. We will specifically document how this duration influences the surface uplift evolution of the landscape and rivers and how the resulting erosional signal is damped and delayed from the initiation of the decrease depending on this duration.

2. Experimental design and procedure

2.1. Experimental design

We studied the erosive response of an experimental landscape subjected to uplift and precipitation. We used a device initially developed at the Geosciences Rennes laboratory (Bonnet and Crave, 2003; Lague et al., 2003; Babault et al., 2005, 2007; Turowski et al., 2006; Bonnet, 2009) but newly installed at the Geosciences Environnement Toulouse laboratory in a modified version, as described below. This device allows us to simulate in the laboratory the development of landscapes formed by erosion induced by runoff of water over a cohesive material. As in previous studies (Bonnet and Crave, 2003, 2006; Babault et al., 2005, 2007; Turowski et al., 2006; Bonnet, 2009), the material used is a silica paste obtained by mixing silica powder (D_{50} = 10–20 μm) with water (20% weight of silica powder). This mixture is homogenized to saturate the porosity of the silica paste and to reduce infiltration phenomena and can then promote sediment transport by surface runoff (Lague et al., 2003). This mixture fills a rectangular box (400 × 600 mm in size and 500 mm in depth), whose base can move upward and downward within the box. The movements of the base are driven by a screw and a stepping motor and are controlled by an automaton. During an experimental run, the base of the box was raised at a constant rate. It pushed the silica outside the top of the box at a rate defined as the uplift rate (U; 1–30 mm/h). Precipitation was generated by a system of four industrial sprinklers that delivered water droplets (diameter < 50 μm) that were small enough to avoid any splash dispersion at the surface of the model, which reduces the action of diffusive hillslope processes (Lague et al., 2003; Sweeney et al., 2015). In the present version of the experimental setup, the water discharge from each sprinkler is controlled by an automaton, which allows precipitation to automatically change during a run. Precipitation was calibrated to be as homogeneous as possible by collecting water in 20 pans at the location of the model. During an experimental run, we used a high-resolution laser sheet (accuracy <0.2 mm) to regularly digitize the surface of the model with a spatial resolution of ~0.5 mm and to produce square-grid digital elevation models. We usually digitized the surface of the models every 5 min, except in the steady state phases when elevations and erosion rates are stable and where digitization intervals can reach 20 min. The erosion rates were computed by dividing the elevation change per pixel between two scans by the time between the scans. Local erosion rates were also averaged to obtain a mean value for the entire landscape.

2.2. Procedure

We present here the results of the experiments where we disturbed an initial topography at a steady state (Fig. 1) by decreasing the precipitation rate from 160 to 60 mm/h, considering different durations of the precipitation decrease (we hereafter referred to this duration as *Tp*). For this purpose, we calibrated nine intermediate fields of precipitation (Table 1). The coefficient of variation of the precipitation rates (standard deviation/mean) is <15% for the experiments carried out here (Table 1). We applied precipitation variations step-by-step rather than by continuously varying the discharge from the sprinklers in order to ensure good quality control of the precipitation history. These steps were of limited duration, usually <60 min; thus, we did not observe any adjustment of the landscape to the individual steps.

We consider here five experiments, one with an instantaneous precipitation decrease ($Tp = 0$) and four with progressive decreases with *Tp* values of 60, 300, 500 and 700 min (Table 2). Then, these experiments were conducted up to a second steady state between erosion and uplift. Fig. 2 shows a schematic evolution of an experiment with $Tp > 0$, which illustrates the terminology used in this paper.

3. Results

3.1. Steady state landscapes

All experiments began with a flat plateau that was uplifted and then progressively dissected by multiple channels that were initiated on the four sides of the model. They formed channel networks that propagated in toward the center of the model, while the mean elevation of the landscape increased (Fig. 1). Under constant uplift and precipitation forcing, the mean and maximum elevations then stabilized, which implies that the erosional flux balanced that of the uplift, thus defining a steady state landscape (SS1). On the basis of experiments presented here (Table 2) and the previous experiments of Babault et al. (2005, 2007), Turowski et al. (2006), Bonnet (2009), and some unpublished experiments, we observe a coevolution of the mean elevation of the experiments at steady state ($<h>_{ss}$) with rainfall and uplift rates (Fig. 3). As already noticed by Bonnet and Crave (2006) using a limited data set, $<h>_{ss}$ is inversely proportional to the precipitation rate (Fig. 3A); however, we observe a large dispersal in the $<h>_{ss}$ values for a given precipitation rate because of the dependency of $<h>_{ss}$ on the uplift rate. Similarly, we observe that $<<h>_{ss}$ is proportional to the uplift rate (Fig. 3B) but that a large dispersal in the $<h>_{ss}$ values occurs because

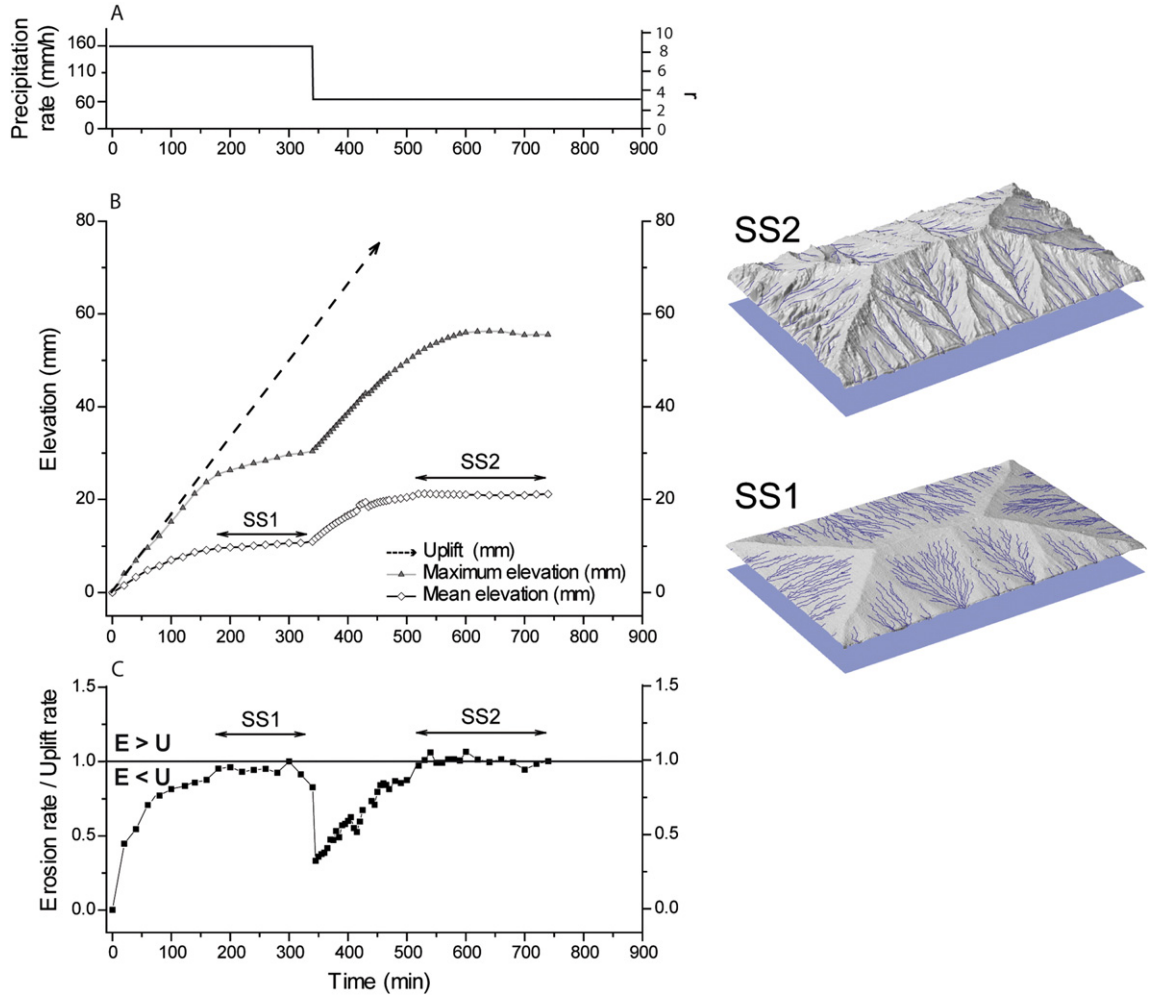

Fig. 1. Evolution of a typical experiment (experiment MOD2) forced by an instant decrease ($Tp = 0$) in the precipitation rate. (A) Precipitation applied and the corresponding water-to-rock ratio (r). (B) Evolution of the mean and maximum elevation. The dotted line indicates the amount of applied uplift, that is, the elevation of the model if no erosion occurred. Periods of constant mean and maximum elevations indicate steady state (erosion rate = uplift rate). (C) Evolution of mean erosion rate (E) of the landscape calculated from mass balance. Erosion rates are normalized to the uplift rate (U). Periods of normalized uplift rates of 1 correspond to steady states. Two examples of steady state landscapes (SS1 and SS2) are shown on the right (three-dimensional view of DEMs; 60 × 40 cm in size).

of the dependency on the rainfall rate. To take into account the covariation of $<h>_{ss}$ with uplift and precipitation, we considered the *water-to-rock ratio* (r) defined by Hasbargen and Paola (2000) and used in subsequent studies (Hasbargen and Paola, 2003; Paola et al., 2009; Reinhardt and Ellis, 2015), which is described as follows:

$$r = \frac{(\rho_w \times P)}{(\rho_s \times U)} \quad (1)$$

Table 1
Precipitation forcing used in this study.

Mean spatial precipitation rate P (mm/h)	Coefficient of variation of precipitation rate (%)	Water-to-rock ratio r
160 ± 23	14	8.4
146 ± 19	13	7.7
129 ± 20	15	6.8
120 ± 14	12	6.3
108 ± 14	13	5.7
100 ± 14	14	5.3
91 ± 10	11	4.8
81 ± 10	12	4.3
75 ± 9	12	3.9
65 ± 10	15	3.4
60 ± 9	15	3.2

where ρ_s is the material density (1.9 g/cm^3), ρ_w is the water density, P is the precipitation rate, and U is the uplift rate. This ratio is a qualitative measure of the erosive efficiency of precipitation compared to uplift (Reinhardt and Ellis, 2015) with low or high values indicating a drier or wetter climate respectively. On the basis of the compilation of 68 values of $<h>_{ss}$, we observe a clear nonlinear inverse dependency of $<h>_{ss}$ as a function of r, with a limited dispersion of the data (Fig. 3C). On a bilogarithmic scale (inset on Fig. 3C), the data align along a line that can be described by the following power law:

$$<h>_{ss} = 42.75.r^{-0.56} \quad (2)$$

In the following section, the effect of the precipitation decrease from 160 to 60 mm/h is investigated using a similar value of U of 10 mm/h in all experiments, which translates into a decrease in r from 8.4 to 3.2 (Table 1). As illustrated in Fig. 3D, the decrease in r should drive a surface uplift of the landscape toward a higher $<<h>_{ss}$. Note that Eq. (2) allows to predict $<h>_{ss}$ for any value of precipitation and uplift forcing and it will be used in the following section to compare the actual evolution of the elevation of the experiments to that of the predicted evolution (using Eq. (2)), assuming that the experiments maintained a steady state during the decrease in precipitation and r. Any departure between the observed and predicted mean elevations of the landscapes

Table 2
Experimental conditions and main parameters derived from elevation and erosion rate histories.

	Tp (min)	Precipitation decrease rate (mm/h)	$<h>_{ss1}$ (mm)	$<h>_{ss2}$ (mm)	Delay, *D* (min)	T_{Emin} (min)	Amplitude *A* (%)	Critical water-to-rock ratio r_c
MOD2	0	instant	10.8	20.4	0	340	67	–
MOD23	60	100	10.6	24.5	31	390	58	5.7
MOD4	300	20	10.9	22.5	200	562	46	4.91
MOD24	500	12	9.8	26.1	300	777	36	5.26
MOD25	700	8.57	10.3	23.4	430	945	24	5.18

will then be used to highlight a disequilibrium state for the experiment, along with a direct comparison between the uplift rate and erosion rate.

3.2. Landscape response to rainfall decrease

3.2.1. Mean elevation histories

As already documented by Bonnet and Crave (2003), an instantaneous decrease in precipitation (*Tp* = 0; Figs. 1 and 4) drives an increase in the mean elevation of the landscape (surface uplift) and then its stabilization to a higher value, which indicates that landscape has recovered to a new steady state (SS2). As already discussed by Bonnet and Crave (2003), the computation of the mean erosion rate indicates that the rainfall decrease actually drives a sudden decrease in the erosion rate, which subsequently increases to recover its steady state value (Fig. 1C). The delay between the precipitation decrease and the recovery to steady state conditions illustrates the response time of the landscape to the precipitation change (Whipple, 2001). It is estimated here of 70.8 ± 2.3 min by fitting an exponential function to the mean elevation curve.

In experiments with *Tp* > 0, a phase of rapid surface uplift to new steady state (SS2) conditions occurred (Fig. 4), the mean elevation of all experiments stabilizing to an average of 23.3 ± 2.1 mm ($<h>_{ss2}$; Table 2), whatever the *Tp*, in agreement with the steady state mean elevation predicted using Eq. (2) (22.7 mm). However, the details of these elevation histories are different. For an experiment with a shorter *Tp* (MOD 23, *Tp* = 60) the surface of the experiment is uplifted at a fast rate (~5.3 mm), very soon after the onset of the precipitation decrease, in a very similar way as in the experiment with *Tp* = 0 (surface uplift of ~5.4 mm/h). This contrasts with the elevation histories of the three experiments with a longer *Tp* that all show a first period of slow surface uplift compared to the imposed uplift rate (surface uplift of ~0.4 mm/h against uplift forcing of 10 mm/h). Then, their elevation departs from this trend, and the topographies uplift at a higher rate before they stabilize and reach the new steady state SS2. The rate of this fast phase of surface uplift decreases with the duration of the precipitation decrease, being 3.4, 2.3, and 1.3 mm/h, respectively, for *Tp* values of 300 (MOD 4), 500 (MOD 24), and 700 min (MOD 25) as seen in Fig. 5B. The onset of this fast surface uplift (T_D, see Fig. 2) also differs between experiments and occurs later for a longer *Tp* (Fig. 4). We observe that the delay between the onset of the precipitation decrease and the onset of the fast phase surface uplift (D on Fig. 2) increases linearly with *Tp* (Fig. 5A).

We show in Fig. 6 the comparison between the observed elevations of the landscapes during the decrease in precipitation and the steady state elevations as predicted using Eq. (2) for any corresponding *r* value. This graph shows that the observed elevations initially match well with the steady state elevations during the progressive decrease in *r*. Then, this graph shows a clear deviation of the observed elevations toward higher values than those of the steady state. These two contrasted situations correspond respectively to the successive periods of slow and fast surface uplift previously described (Fig. 4). This indicates that the landscape constantly remains at a steady state during the slow surface uplift period, its mean elevation being constantly adjusted to the decrease in precipitation and *r*. Hereafter, we will refer to this period as a Transient Steady state (TSS in Fig. 2).

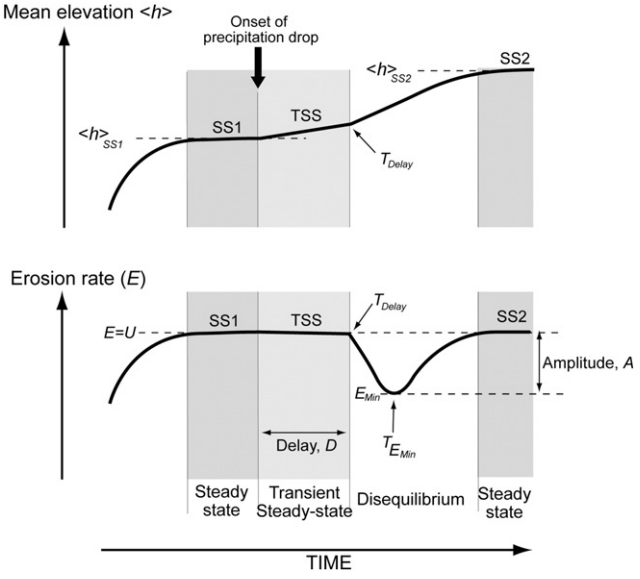

Fig. 2. Schematic evolution of an experiment forced by a finite decrease in the precipitation rate (*Tp* > 0) illustrating the terminology used in this study. SS1: steady state 1; SS2: steady state 2; TSS: transient steady state; $<h>_{SS1}$: mean elevation at SS1; $<h>_{SS2}$: mean elevation at SS2; *D*: delay between the onset of the precipitation decrease and the onset of the geomorphic and erosional response. T_{Delay}: Time at the onset of the geomorphic and erosional response; E_{min}: minimum erosion rate at disequilibrium; *A*: amplitude of the decrease in the erosion rate; T_{Emin}: time at E_{min}.

3.2.2. River profile histories and knickpoint propagation

The longitudinal profiles of landscapes at steady state with regard to high and low precipitation and *r* values are characterized by different concavities, estimated from the exponents of slope-area relationships (Flint, 1974) to be 0.07 (SS1) and 0.2 (SS2) respectively. These values are low compared to those of natural rivers (e.g., Kirby and Whipple, 2012) but are in the range of the exponents classically observed in such experiments (0.05–0.3; see discussion below and in Lague et al., 2003; Bonnet and Crave, 2006; Singh et al., 2015). For the experiments here, the temporal sequences of the longitudinal profiles, which are shown here every 20 min for clarity (Fig. 7), also reveal different evolutionary histories (as for mean landscape elevation) according to *Tp*. A schematic illustration of the evolution of the longitudinal profiles is shown in Fig. 7F for clarity. Globally, the disruption of the SS1 landscape by a precipitation decrease sets the uplift of the former (SS1) longitudinal profiles and the migration of a knickpoint until a new steeper equilibrium profile (SS2) is reached with a higher concavity value, following the mechanism described by Whipple and Tucker (1999) from analytical modeling. Notably in all the experiments, the downstream ends of the profiles always remained pinned to the borders of the erosion box, representing the base-level for erosion. We never observed any major surface uplift in the downstream ends of the profiles and their disconnection relative to base level. During knickpoint propagation, the upstream segment retains its initial shape inherited from the SS1 period, while the downstream segment gradually steepens to the final steady state SS2 profile.

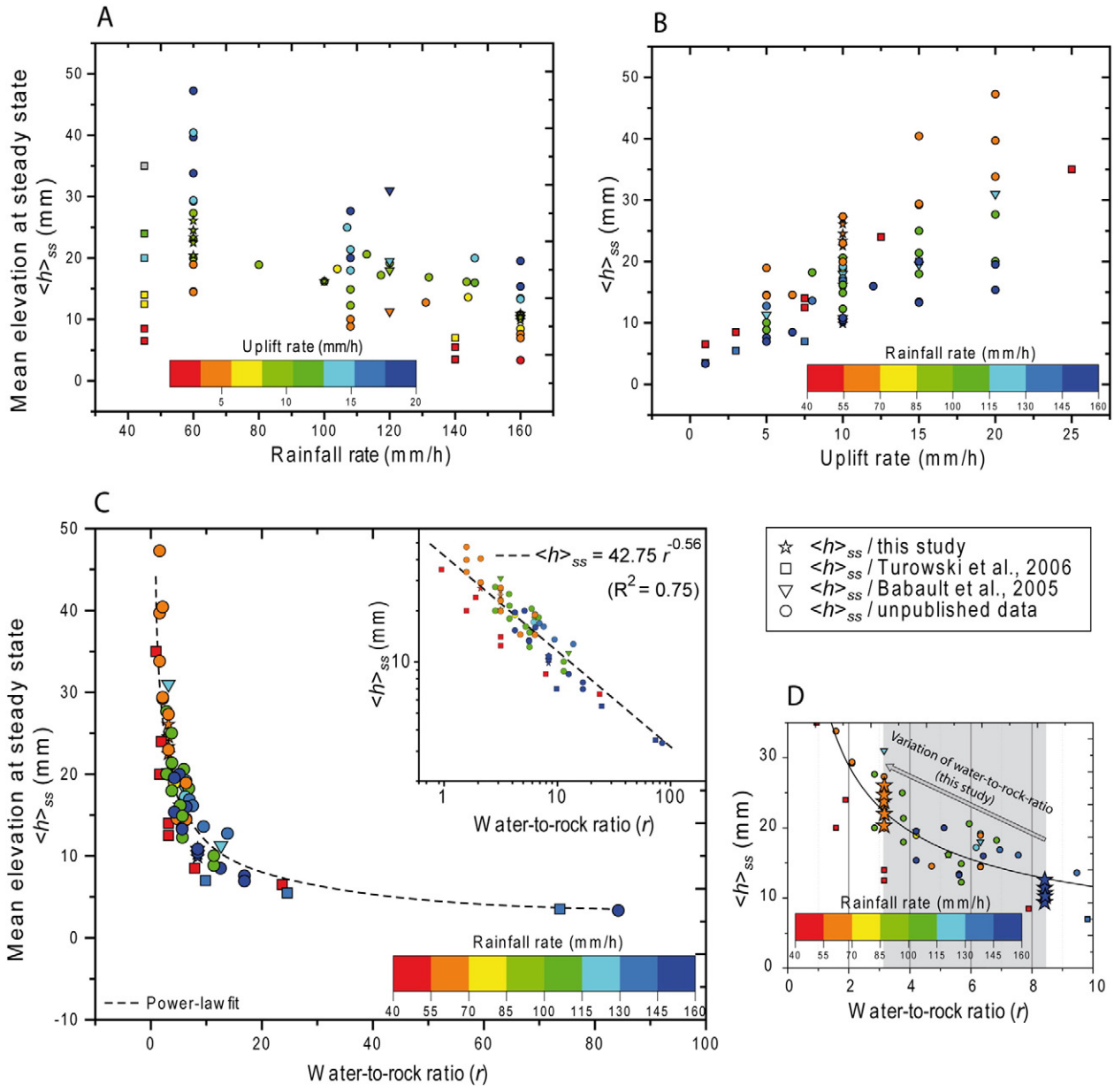

Fig. 3. Compilation of mean elevations of experimental landscapes at steady state, from this study, bibliography, and unpublished data showing the relationship with precipitation rate (A), uplift rate (B), and water-to-rock ratio (C). Graph in D is an enlargement of graph C that shows the decrease in the water-to-rock ratio (8.4 to 3.2) considered in this study (gray area) and the expected change in the steady state mean elevation of the landscapes.

For the experiment with an instantaneous decrease ($Tp = 0$; Fig. 7A), knickpoints are initiated immediately after the variation in the rainfall rate. However, for three of the experiments with $Tp > 0$ ($Tp = 60$, 300, and 500 min: Fig. 7) the longitudinal profiles first rise slightly while maintaining overall their initial concavity, and knickpoints initiate and propagate only during a second phase. This first period coincides with the slow surface uplift period and TSS previously described. The onset of knickpoint propagation is not synchronous in all the experiments (Fig. 8) but occurs after a long delay (D, Fig. 2) for the longer Tp. Notably although the rate of surface uplift depends on Tp (Figs. 3 and 5B), the rate of knickpoint propagation is similar in all experiments, at ~150 mm/h. Finally, this peculiar evolution of the longitudinal profiles is not well defined for the experiments with a longer Tp (Fig. 7E), as a propagating knickpoint is not clearly visible. The sequence of longitudinal profiles rather shows a gradual evolution between the two steady state profiles.

3.2.3. Erosion rate histories

The erosion rates for an experiment with an instantaneous decrease ($Tp = 0$) show the typical evolution described previously (Fig. 1) and already observed by Bonnet and Crave (2003). A precipitation decrease drives a strong decrease in the mean erosion rate (Fig. 9A), which represents here ~67% of the uplift rate value (Fig. 5C, Table 2). Then erosion rate progressively increases, whereas topography is progressively uplifted and the system finally recovers to a steady state (SS2), as the erosion rate balances the uplift rate. For experiences with a longer Tp, we also observed this decrease in erosion rate; however, it occurred after a period where erosion rates remained close to those of uplift (Fig. 9B–E). This corresponds to the period of slow surface uplift and TSS described in the mean elevation histories. Then, only after the delay D discussed previously (see also Fig. 2) did the erosion rate decrease significantly, with the onset of the erosion decrease occurring later for a longer Tp. The comparison between all the experiments

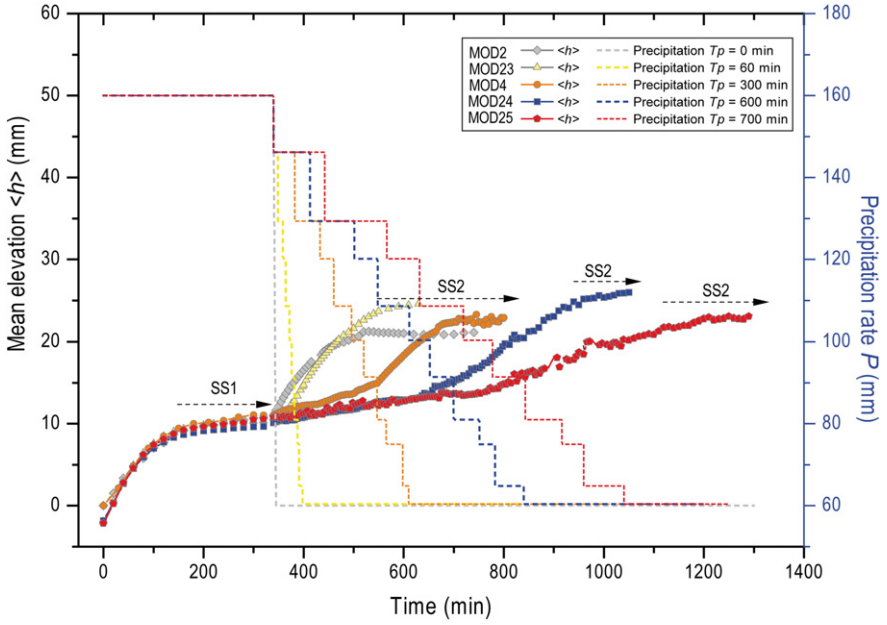

Fig. 4. Mean elevation histories of experiments performed in this study and associated precipitation forcing. The uplift rate is the same for all the experiments (10 mm/h).

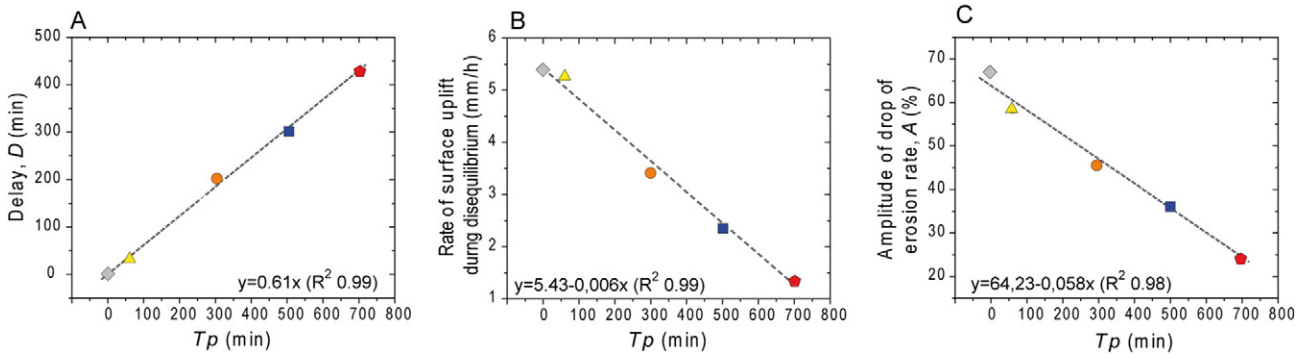

Fig. 5. Delay (A), rate of surface uplift during disequilibrium (B) and amplitude of the decrease in the erosion rate expressed by the amplitude (%) of its departure from steady state (C). Symbols are the same as in Fig. 4.

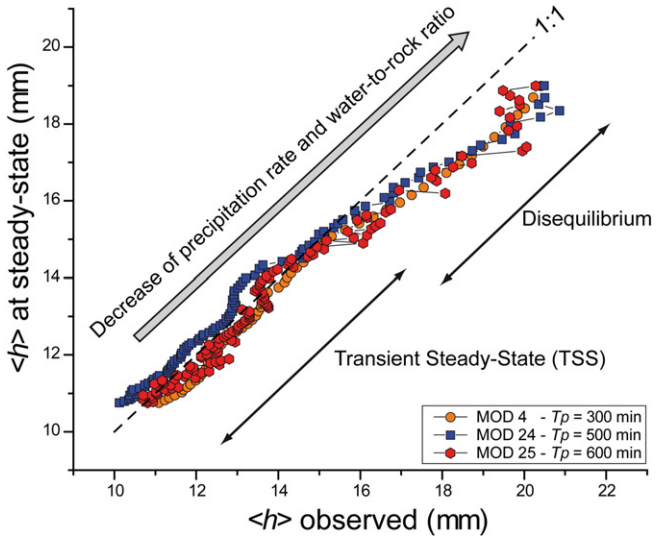

Fig. 6. Mean elevation of the landscapes observed during a precipitation decrease compared to the predicted mean elevation at steady state related to the decrease in the water-to-rock ratio as calculated using Eq. (2). See text for comments.

then illustrated that the erosional response is delayed with regard to the onset of the change in precipitation, whether considering the onset of the erosion decrease or the minimum erosion rate (E_{min} on Fig. 2). The amplitude of the decrease in the mean erosion rate (A on Fig. 2) also differs between experiments, i.e., with Tp (Fig. 9, Table 2). In the experiment with an instantaneous decrease, the minimum mean erosion rate is ~3 mm/h, representing a departure from the uplift rate of ~67%, whereas for the longest Tp, the minimum mean erosion rate is approximately 8 mm/h, representing a departure from the uplift rate of only 24%. The amplitude of the decrease in the erosion rate decreases linearly with Tp (Fig. 5C), which indicates that the erosional response is damped for a longer Tp.

3.2.4. Evidence of a geomorphic threshold related to critical rainfall and water-to-rock ratio

The response of the experiments to a rainfall decrease in terms of elevation and erosion rate histories and the longitudinal profile evolution is characterized by a delay between the onset of the precipitation decrease and the onset of these responses at the end of the TSS. Given the rates of the precipitation decreases, we used the delay D (Table 2) of each experiment to determine the value of the precipitation rate and r at the end of the TSS. We observe that the end of the TSS coincides

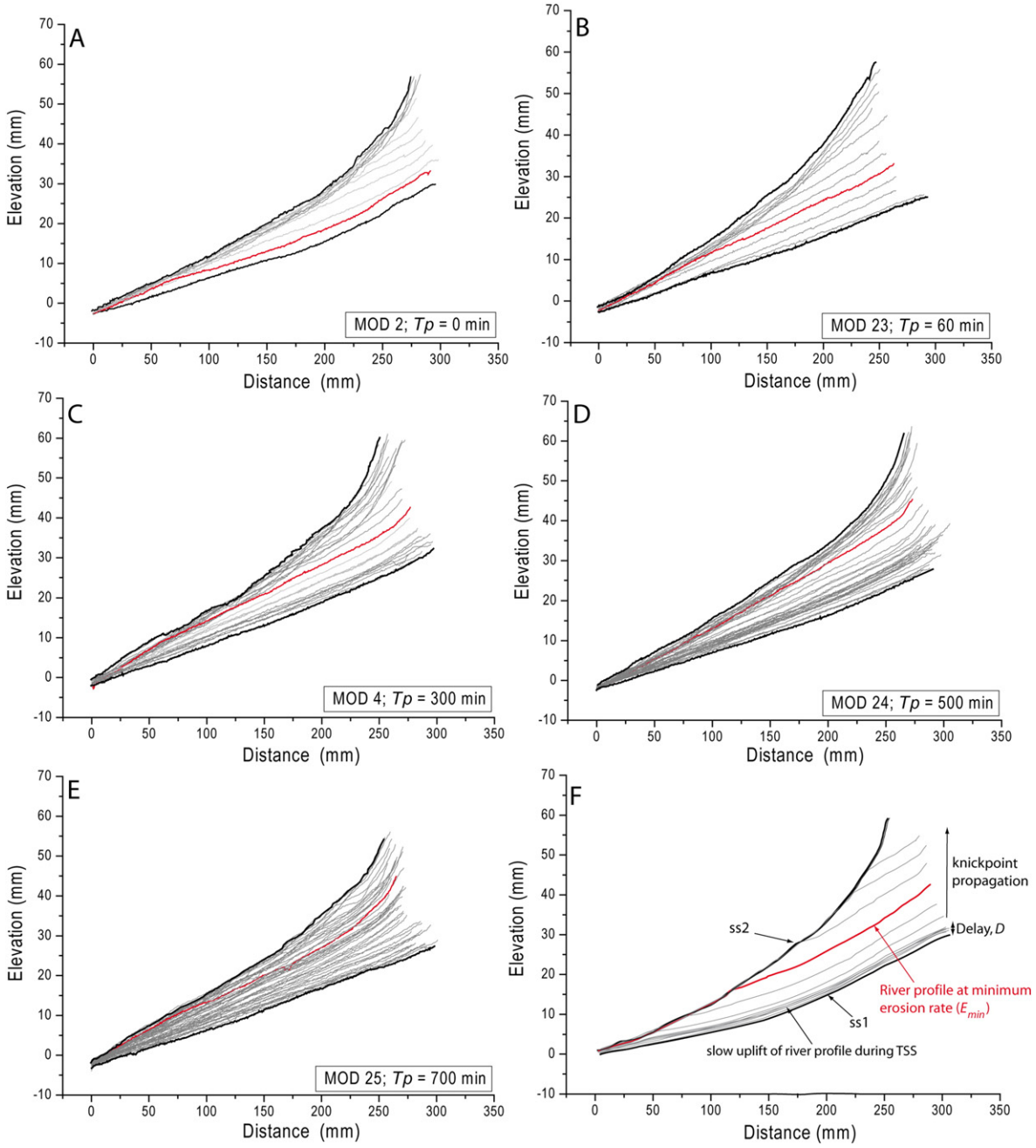

Fig. 7. (A)–(E): Sequence of evolution of the longitudinal profiles during a precipitation decrease, from SS1 to SS2 (time interval between each profile is 20 min). Profiles in (F) are schematic and are shown here to guide the interpretation.

with very similar values for precipitation rate and r, with average values of 99.7 ± 6.2 mm/h and 5.3 ± 0.3 respectively (Fig. 10). Hence, this indicates that the landscape response to the precipitation variation is controlled by a critical value of the precipitation rate and r (hereafter referred to as critical r, r_c: Table 2). Before crossing this value, during the TSS period, the landscapes keep pace with decreasing precipitation and an equilibrium is maintained. Then, once r_c is crossed, the landscape is in disequilibrium and is uplifted much faster than if it remained at a steady state with a decreasing r (e.g., Fig. 6) and a decrease in the erosion rate observed. This critical value r_c then controls the time at which disequilibrium occurs. Given that we considered linear decreases in precipitation, this explains why the resulting time lag increases linearly with the duration of the decrease (Fig. 5A).

Our data show that once the critical rainfall and the corresponding r_c are crossed, the longitudinal profiles depart from the steady state and are passively uplifted while knickpoints initiate at their downstream ends and propagate upward (Fig. 7). This suggests that the landscape response to the precipitation decrease involves a geomorphic threshold. The nature of this threshold can be discussed on the basis of slope-area data of experiments (Fig. 11). At high r values, slope-area data of steady state landscapes show a unique linear trend in log-log coordinates for areas >5–10 mm^2, with a low concavity exponent value of ~0.1 or less. The corresponding longitudinal profiles are almost linear (profiles at SS1 in Fig. 7). In contrast, all steady state experiments with a low r value show a disruption of this trend at areas of ~50–100 mm^2 (Fig. 11), with a higher concavity exponent downward of ~0.15–0.20.

Longitudinal profiles at SS2 shown in Fig. 7 correspond to this domain with a higher concavity. The development of this domain of higher concavity coincides with the initiation of knickpoint migration at the end of the TSS period and to the time when the critical rainfall and r_c are crossed. This suggests that these critical values correspond to a geomorphic transition and are likely related to a change in the processes of erosion and transport acting on the experiments (see below).

4. Interpretation and discussion

4.1. Importance of a rainfall-related geomorphic threshold on the macroscale dynamics of landscapes

At high precipitation and r values, landscapes are characterized by very low concavity channels, with concavity of ~0.1 or less. Such very low concavity channels are classically observed in similar experiments (Hasbargen and Paola, 2003; Lague et al., 2003; Bonnet and Crave, 2006; Singh et al., 2015) and may correspond to unchanneled valleys by reference to natural systems (e.g., Montgomery and Foufoula-Georgiou, 1993). In contrast, once r_c is crossed, channels with larger concavity, of ~0.15–0.20, developed during the transient phase TSS. These larger-concavity channels are characteristic of steady state landscapes under low precipitation and r values. Channels with concavity in the range of 0.15–0.30 are classically observed in experimental landscapes and are interpreted as channels shaped by fluvial-like processes (Hasbargen and Paola, 2003; Lague et al., 2003; Bonnet and Crave, 2006; Singh et al., 2015) even if fluvial channels in nature typically show concavity ranging from 0.40 to 0.60 (e.g., Kirby and Whipple, 2012). However, designs used in the experimental modeling of landscapes have never succeeded in producing channels with this exact range of concavity values. Here, we propose that the critical value of the water-to-rock ratio r_c corresponds to a transition from unchanneled valleys to fluvial channels driven by the onset of fluvial channelization.

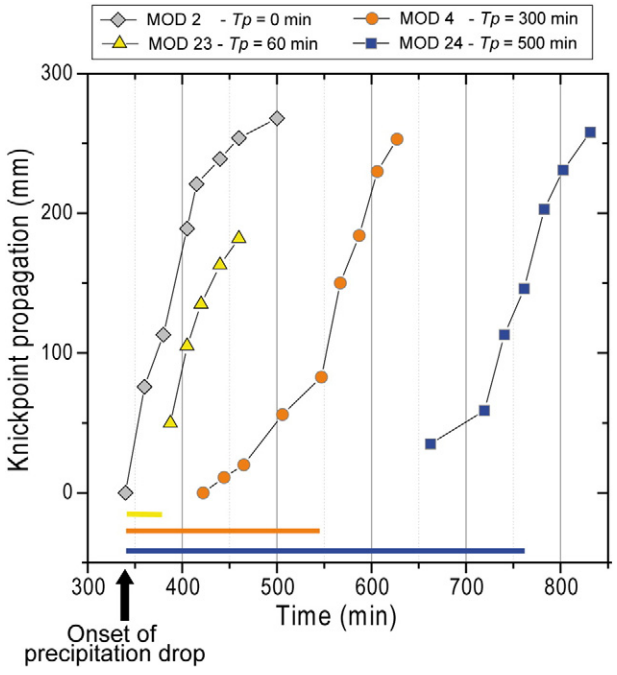

Fig. 8. Pattern of knickpoint propagation over time for experiments with *Tp* values between 0 and 500 min. Experiment completed with $Tp = 700$ min does not show a clear propagation of knickpoints (Fig. 7E) and is consequently not shown here. Color bars at the bottom of the graph show the delay D for each experiment. This illustrates that knickpoints start to propagate at the end of the transient steady state period. Note that the pattern and rate of knickpoint propagation are very similar between all experiments.

The issue of channel initiation has long been acknowledged to be a major issue in understanding the landscape response to climate variations (e.g., Montgomery and Dietrich, 1992; Rinaldo et al., 1995; Tucker and Slingerland, 1997). The location of channel heads may be defined by the competition between diffusive and advective transport processes (Smith and Bretherton, 1972; Perron et al., 2009; Sweeney et al., 2015) or by the existence of a geomorphic threshold for runoff erosion related to shear stress (Horton, 1945; Montgomery and Dietrich, 1992). Because diffusive hillslope processes are of a limited extent in the type of experiments used here (Lague et al., 2003; Sweeney et al., 2015), the competition between diffusive and advective processes is unlikely to be the main driver of the geomorphic transition that was observed. We consequently consider that the transition from unchanneled valleys to fluvial channels is controlled here by a threshold of channelization. Given the importance of this transition in the dynamics of the experimental landscape, however, this specific issue will require further investigation.

In our experiments, steady state landscapes characterized by unchanneled valleys (high water-to-rock ratio) or fluvial channels (low water-to-rock ratio) differ in their macroscopic properties, such as their mean elevation at steady state. During a precipitation decrease, the change in the process from unchanneled valleys to fluvial channels corresponds to a threshold that is controlled by a critical water-to-rock ratio; this change is the main mechanism that imprints a signature in terms of mean elevation and erosion rate histories. It drives a transient period of incision propagation through knickpoints, which coincides with a decrease in the mean erosion rate of the landscape and consequently its surface uplift. The applicability of this finding to natural landscapes is not straightforward because a complete scaling of experimental landscapes is intractable because of inescapable scale distortions between experiments and nature (see discussions in Bonnet and Crave, 2003, 2006; Lague et al., 2003; Bonnet, 2009; Singh et al., 2015; Sweeney et al., 2015; as well as Paola et al., 2009, for a thorough review of scaling problems in experimental geomorphology). Despite scaling problems, slope-area data can be used, however, to suggest some analogies between experimental and natural landscapes (Bonnet and Crave, 2006). Trends observed on power law plots of slope versus drainage area from landscape experiments (e.g., Fig. 11) are very similar to those observed on natural landscapes (for example, compare the slope-area trends of SS2 (Fig. 11) with Fig. 4 of Montgomery and Foufoula-Georgiou (1993) or Fig. 1 of Ijjasz-Vasquez and Bras (1995)). The inflection observed here at ~100 mm^2 (SS2 on Fig. 11; Bonnet and Crave, 2006) occurs in nature for critical drainage areas of 0.1 to 5 km^2 (Montgomery and Foufoula-Georgiou, 1993; Ijjasz-Vasquez and Bras, 1995; Stock and Dietrich, 2003; Kirby and Whipple, 2012; D'Arcy and Whittaker, 2014; Lague, 2014). On the basis of this analogy, we can assume to a gross approximation that the drainage basins in our experiments (maximum drainage area of ~20,000 mm^2; Fig. 11) represent natural drainage basins with sizes of 20 to 1000 km^2, i.e., with lengths of 4.5 to 30 km, by considering a classic empiric law between drainage basin length and area (e.g., Montgomery and Dietrich, 1992). If we consider a two-side landscape, this indicates that our landscape experiments could be viewed as analogs of topographic ranges with a width of some tens of kilometers, which is typically the size of uplifted blocks observed in basin-and-range-like topographies, in compressional and extensional settings (Hovius, 1996; Talling et al., 1997). Then, our experiments do not pretend to represent the evolution of a landscape of whole mountain belts and their related drainage networks but rather smaller-scale topographic features. However, these ranges are important in setting the geophysical relief of an area (Champagnac et al., 2012) and in delivering sediments to large river systems. These natural landscapes are typical places where the dynamics that we described here and their signatures (e.g., knickpoints between unchanneled valleys and fluvial channels) should be investigated in future studies.

4.2. A damped and delayed erosional response to long-term precipitation variations: implications

Our study illustrates the damping of the erosional response to a precipitation decrease according to the duration *Tp* of the climatic perturbation (Fig. 9) with an amplitude of the departure of the erosion rate from its steady state value that decreases from 67% for instant perturbation to only 23% for the longer *Tp* tested here (Fig. 5C). From the data shown in Fig. 5C, we can reasonably speculate that an experiment completed with a longer *Tp*, of ~1100 min here, should not show any significant departure in the erosion rate from its steady state value imposed by the uplift rate. Such a lack of erosional response to long-term climatic variations has already been inferred from numerical simulations of landscape responses to cyclic rainfall variations by Godard et al. (2013) and Braun et al. (2015). Using a landscape evolution model that simulates hillslope and fluvial processes, Godard et al. (2013) observed that the departure in the erosion rate from the uplift rate approaches zero for oscillation periods of rainfall that are on the order of hundreds of thousands of years to millions of years, depending on erodibility. The same conclusion has been addressed by Braun et al. (2015) using analytical solutions of the stream power law, with a response amplitude that approaches zero for long forcing periods of longer than one million years, regardless of the *m* and *n* values of the exponents of the stream power law that was considered. Here, we cannot physically scale our experiments and experimental transfer times into time in natural landscapes (see discussions in Bonnet and Crave, 2006, and Paola et al., 2009); however, by comparison to results obtained from numerical modeling, we consider that the damped effects that we document should probably be applied to natural systems for long-term (10^5 to 10^6 years) climatic variations and not at the scale of shorter Milankovitch-controlled climatic cycles, for example. The damping effect that we document is observed for durations of rainfall decrease in *Tp* that are significantly longer than the response time of the landscape to abrupt rainfall variations (~150 min in the experiment shown in Fig. 1), which also indicates that we are documenting processes that would likely occur on million-year time scales in natural systems. Actually, even if the response time of landscapes is critically unknown in nature, there is general agreement that it is rather a question of million(s) of years (Whipple and Meade, 2006). Thus, we propose that the damping effect that we document could occur in nature in response to long-term climate change, such as the long-term climatic evolution that characterized the Cenozoic, for example (Zachos et al., 2001). As already noted by Braun et al. (2015), this implies that long-term variations in precipitation may have a weak impact on the erosion of landscapes and on the delivery of siliciclastic material to large rivers and sedimentary basins. This indicates in particular that the ability of sediment archives to record changes in precipitation, such as those related to monsoon development, for example (Clift et al., 2014), critically

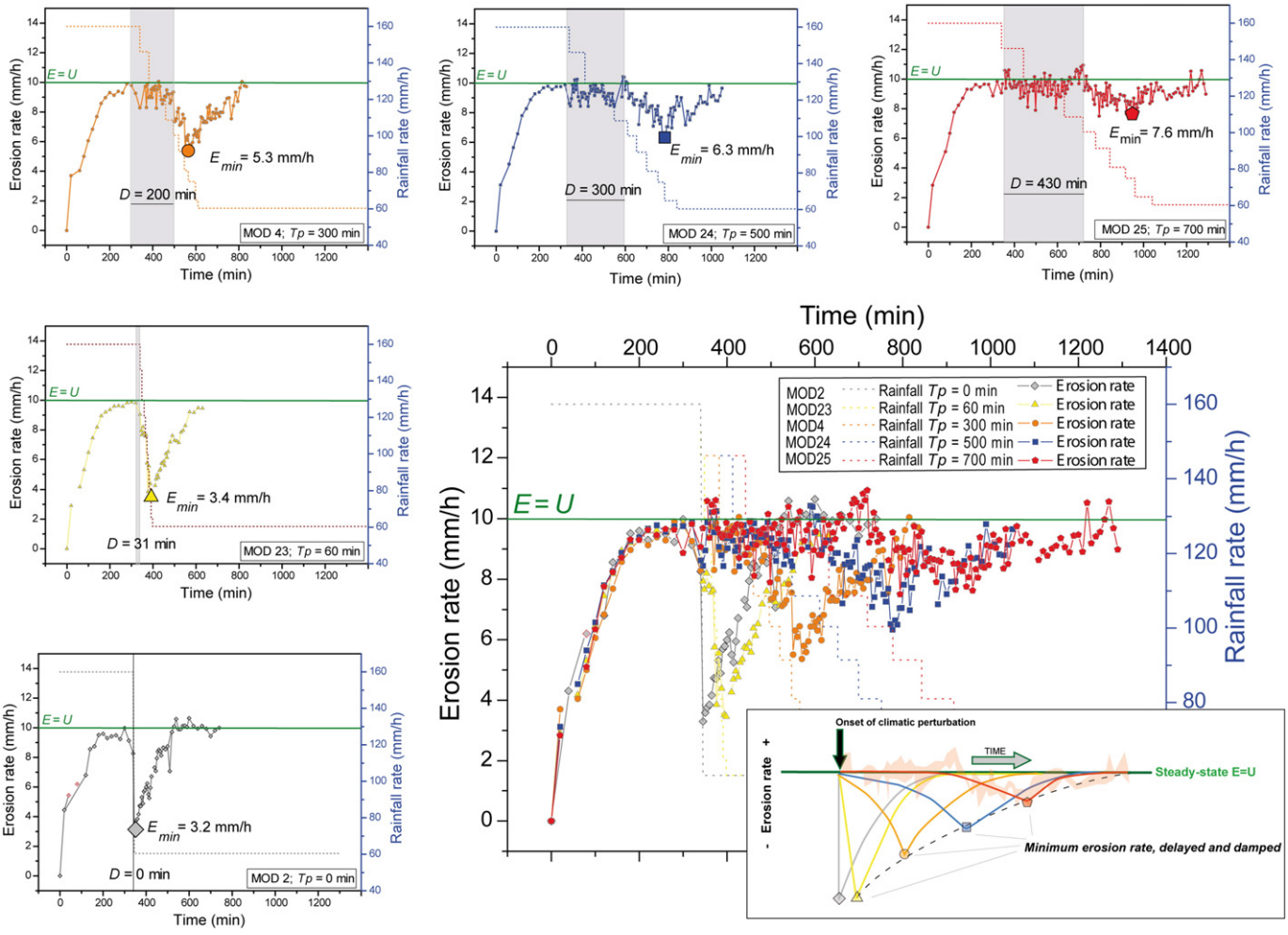

Fig. 9. Mean erosion rates (E) calculated from mass balance. Green line indicates the uplift rate (U) used in these experiments (10 mm/h). Periods with $E = U$ correspond to steady state conditions. In experiments with $Tp > 0$, the departure of the erosion rate from its steady state value occurs after a delay D (gray area) compared to the onset of the precipitation decrease (at 340 min). The duration of D increases with Tp (see also Fig. 5A). At disequilibrium, the amplitude (A) of the decrease in the erosion rate (minimum erosion rate E_{min}) decreases with Tp (see also Fig. 5C), showing a damping of the erosional signal according to the duration of the precipitation decrease Tp. Note that the time when the erosion rate is at a minimum also depends on Tp, which also indicates a delayed response.

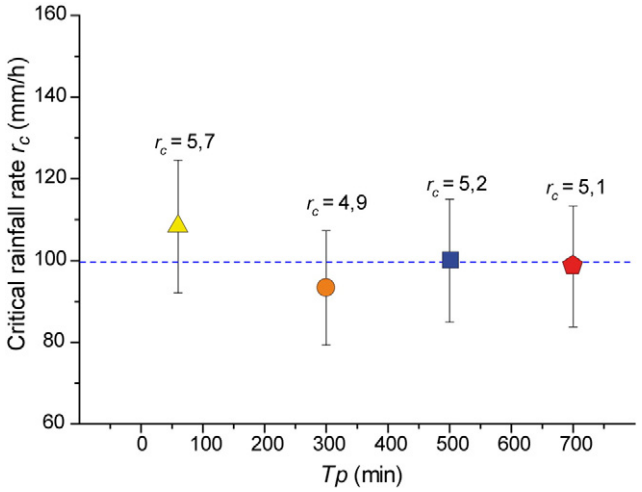

Fig. 10. Precipitation rate at the transition between the transient steady state and disequilibrium phases (T_{Delay} on Fig. 2) for an experiment with $Tp > 0$. Also shown is the corresponding value of the water-to-rock ratio, r_c (see text).

depend on the time scale of the variations, with brief intensification events being more liable to produce an erosional response. This finding is important for interpreting the terrigenous supply from continents to oceans at geological time scales (10^{6-7} years) as gathered from clastic volumes preserved in sedimentary basins (e.g., Leturmy et al., 2003; Rouby et al., 2009; Guillocheau et al., 2012; Grimaud et al., 2017). Notably, however, although long-term precipitation variations may weakly influence erosion rate values, they do impact the elevation of landscapes. Thus, we can speculate that long-term climate change, through precipitation, may impact the state of stress of an orogen and consequently impact its tectonic evolution through variations in its topography, without any major or detectable variations in its erosion rates.

Another important outcome of our study is that the erosional response to a precipitation decrease is delayed with regard to the onset of the precipitation perturbation. In our experiments, this delay exists because the geomorphic response to the changing climate is controlled by a threshold. Before crossing this threshold, the landscape continuously adjusts to the changing climate during a transient steady state period. The duration of this period, i.e., of the delay, depends on the time scale of the precipitation decrease. A time lag between a tectonic or climatic forcing and its geomorphic response is observed in numerical simulations (e.g., Kooi and Beaumont, 1996; Braun et al., 2015) in the case of periodic forcing variations when the periodicity of forcing is close to the response time of the geomorphic system. Actually, if the periodicity of forcing is longer, then the system always remains at equilibrium (the 'reactive landscape' of Allen, 2008). In contrast, the system never fully adjusts to forcing and always remains out of equilibrium ('buffered landscape' of Allen, 2008). Consequently, for 'intermediate' forcings (Kooi and Beaumont, 1996), a time lag between forcing and response may exist. In our experiments here, the time lag is not related to a similar mechanism but to the existence of a geomorphic threshold that dictates the timing of the onset of the geomorphic and erosional responses during the ongoing variation in precipitation. However, as has already been noted by Allen (2008), this suggests that great caution must be taken when one aims to infer the timing of a climatic event on the basis of the age of its sedimentary response.

5. Conclusions

We investigated the landscape and erosive responses to climate change in laboratory experiments by considering the response of landscapes already at steady state to precipitation decreases of different durations. We observed in all our experiments that a decrease in the precipitation rate, regardless of its duration, drives the uplift of the landscape from an initial steady state mean elevation value to a higher elevation, according to the corresponding change in the forcing as expressed by the water-to-rock ratio. However, the transient histories are very different between experiments. On the one hand, experiments with a sudden decrease in precipitation show a transient phase of disequilibrium that is initiated immediately after the decrease. As already described by Bonnet and Crave (2003), it is characterized by surface uplift of the landscape, the propagation of knickpoints, and a strong decrease in the erosion rate. On the other hand, in the experiments forced by a finite duration of the precipitation decrease, this phase of disequilibrium only occurs after a first period, defined here as a transient steady state (TSS) period, when the landscape remains at a steady state despite the lowering of the precipitation rate and the related water-to-rock ratio. A response is observed in terms of surface uplift or of departure of the erosion rate from its steady state value only when a critical value of the precipitation rate and the rainfall-to-rock ratio are crossed. Our data suggest that this critical value corresponds to a threshold that controls a change in the transport processes acting on the landscape. We observed that the landscape and erosional responses to a precipitation decrease are delayed compared to the onset of the decrease in precipitation. We also observed that the amplitude of the decrease in the erosion rate decreases according to the duration of the precipitation decrease, which indicates a damping of the erosional signal. This suggests that long-term variations in precipitation may have a weak impact on the erosion of landscapes and on the delivery of siliciclastic material to large rivers and sedimentary basins.

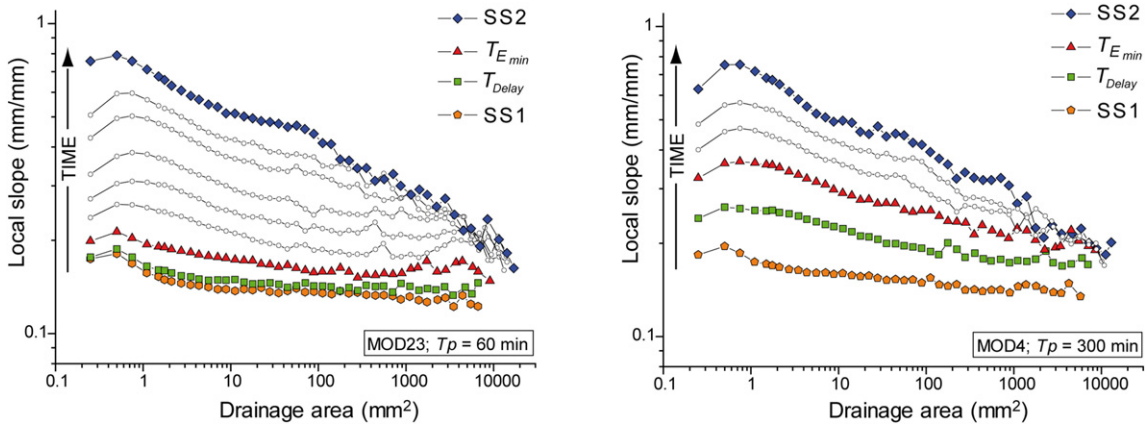

Fig. 11. Log-log plots of slope-area data for selected steps (see Fig. 2) in the evolution of experiments MOD23 and MOD4 and some intermediate steps (open symbols) between T_{Emin} and SS2. See text for comments.

Acknowledgements

Stéphane Bonnet thanks the CNRS-INSU, the University Paul Sabatier/Toulouse III, Géosciences Environnement Toulouse (GET), and the Observatoire Midi-Pyrénées for their financial support during the development at Toulouse of the new experimental facility used in this study. We thank two anonymous reviewers and the editor Richard Marston for their constructive comments.

References

Allen, P.A., 2008. Time scales of tectonic landscapes and their sediment routing systems. In: Gallagher, K., Jones, S.J., Wainwright, J. (Eds.), Landscape evolution: denudation, climate and tectonics over different time and scape scales. Geological Society, London, Special Publications 296, pp. 7–28.

Babault, J., Bonnet, S., Crave, A., Van den Driessche, J., 2005. Influence of piedmont sedimentation on erosion dynamics of an uplifting landscape: an experimental approach. Geology 33, 301–304.

Babault, J., Bonnet, S., Van den Driessche, J., Crave, A., 2007. High elevation of low-relief surfaces in mountain belts: does it equate to post-orogenic surface uplift? Terra Nova 19, 272–277.

Bonnet, S., 2009. Shrinking and splitting of drainage basins in orogenic landscapes from the migration of the main drainage divide. Nat. Geosci. 2, 766–771.

Bonnet, S., Crave, A., 2003. Landscape response to climate change: insights from experimental modeling and implications for tectonic versus climatic uplift of topography. Geology 31, 123–126.

Bonnet, S., Crave, A., 2006. Macroscale dynamics of experimental landscapes. Geol. Soc. Lond. Spec. Publ. 253, 327–339.

Bookhagen, B., Burbank, D.W., 2006. Topography, relief, and TRMM-derived rainfall variations along the Himalaya. Geophys. Res. Lett. 33, L08405. https://doi.org/10.1029/2006GL026037.

Bookhagen, B., Strecker, M.R., 2012. Spatiotemporal trends in erosion rates across a pronounced rainfall gradient: examples from the southern Central Andes. Earth Planet. Sci. Lett. 327–328, 97–110.

Braun, J., Voisin, C., Gourlan, T., Chauvel, C., 2015. Erosional response of an actively uplifting mountain belt to cyclic rainfall variations. Earth Surf. Dyn. 3, 1–14.

Burbank, D.W., Blythe, A.E., Putkonen, J., Pratt-Sitaula, B., Gabet, E.J., Oskin, M., Barros, A.P., Ojha, T.P., 2003. Decoupling of erosion and precipitation in the Himalayas. Nature 426, 652–655.

Carretier, S., Regard, V., Vassallo, R., Aguilar, G., Martinod, J., Riquelme, R., Pepin, E., Charrier, R., Hérail, G., Farías, M., Guyot, J.L., Vargas, G., Lagane, C., 2013. Slope and climate variability control of erosion in the Andes of central Chile. Geology 41, 195–198.

Champagnac, J.D., Molnar, P., Sue, C., Herman, F., 2012. Tectonics, climate, and mountain topography. J. Geophys. Res. 117. https://doi.org/10.1029/2011JB008348.

Clift, P.D., Wan, S., Blusztajn, J., 2014. Reconstructing chemical weathering, physical erosion ad monsoon intensity since 25 Ma in the northern South China Sea: a review of competing proxies. Earth Sci. Rev. 130, 86–102.

Dahlen, F.A., Suppe, J., Davis, D., 1984. Mechanics of fold-and-thrust belts and accretionary wedges: cohesive coulomb theory. J. Geophys. Res. 89, 10087–10101.

D'Arcy, M., Whittaker, A.C., 2014. Geomorphic constraints on landscape sensitivity to climate in tectonically active areas. Geomorphology 204, 366–381.

Deeken, A., Thiede, R.C., Sobel, E.R., Hourigan, J.K., Strecker, M.R., 2011. Exhumational variability within the Himalaya of northwest India. Earth Planet. Sci. Lett. 305 (1–2), 103–114.

Flint, J.J., 1974. Stream gradient as a function of order, magnitude, and discharge. Water Resour. Res. 10, 969–973.

Godard, V., Tucker, G.E., Fisher, G.B., Burbank, D.W., Bookhagen, B., 2013. Frequency-dependent landscape response to climatic forcing. Geophys. Res. Lett. 40, 1–5.

Godard, V., Bourlès, D.L., Spinabella, F., Burbank, D.W., Bookhagen, B., Burch Fisher, G., Moulin, A., Léanni, L., 2014. Dominance of tectonics over climate in Himalayan denudation. Geology 42, 243–246.

Grimaud, J.-L., Rouby, D., Chardon, D., Beauvais, A., 2017. Cenozoic sediment budget of West Africa and the Niger delta. Basin Res. https://doi.org/10.1111/bre.12248.

Guillocheau, F., Rouby, D., Robin, C., Helm, C., Rolland, N., Le Carlier de Veslud, C., Braun, J., 2012. Quantification and causes of the terrigeneous sediment budget at the scale of a continental margin: a new method applied to the Namibia-South Africa margin. Basin Res. 24, 3–30.

Hasbargen, L.E., Paola, C., 2000. Landscape instability in an experimental drainage basin. Geology 28, 1067–1070.

Hasbargen, L.E., Paola, C., 2003. How predictable is local erosion rate in eroding landscapes? In: Wilcocp, P.R., Iverson, R.M. (Eds.), Prediction in Geomorphology. Geophysical. Monograph. 135. American Geophysical Union, Washington, D.C., pp. 231–240

Herman, F., Seward, D., Valla, P.G., Carter, A., Kohn, B., Willett, S.D., Ehlers, T.A., 2013. Worldwide acceleration of mountain erosion under a cooling climate. Nature 504. https://doi.org/10.1038/nature12877.

Horton, R.E., 1945. Erosional development of streams and their drainage basins: hydrological approach to quantitative morphology. Geol. Soc. Am. Bull. 56, 275–370.

Hovius, N., 1996. Regular spacing of drainage outlets from linear mountain belts. Basin Res. 8, 29–44.

Ijjasz-Vasquez, E.J., Bras, R.L., 1995. Scaling regimes of local slope versus contributing area in digital elevation models. Geomorphology 12, 299–311.

Kirby, E., Whipple, K.X., 2012. Expression of active tectonics in erosional landscapes. J. Struct. Geol. 44, 54–75.

Kooi, H., Beaumont, C., 1996. Large-scale geomorphology: classical concepts reconciled and integrated with contemporary ideas via a surface process model. J. Geophys. Res. 101 (3361-2286).

Lague, D., 2014. The stream power river incision model: evidence, theory and beyond. Earth Surf. Process. Landf. 39, 38–61.

Lague, D., Crave, A., Davy, P., 2003. Laboratory experiments simulating the geomorphic response to tectonic uplift. J. Geophys. Res. Solid Earth 108. https://doi.org/10.1029/2002JB001785.

Leturmy, P., Lucazeau, F., Brigaud, F., 2003. Dynamic interactions between the gulf of Guinea passive margin and the Congo River drainage basin: 1.Morphology and mass balance. J. Geophys. Res. 108, 2156–2202.

Montgomery, D.R., Dietrich, W.E., 1992. Channel initiation and the problem of landscape scale. Science 255, 826–830.

Montgomery, D.R., Foufoula-Georgiou, E., 1993. Channel network source representation using digital elevation models. Water Resour. Res. 29, 3925–3934.

Moon, S., Page Chamberlain, C., Blisniuk, K., Levine, N., Rood, D.H., Hilley, G.E., 2011. Climatic control of denudation in the deglaciated landscape of the Washington cascades. Nat. Geosci. 4, 469–473.

Paola, C., Straub, K., Mohrig, D., Reinhardt, L., 2009. The "unreasonable effectiveness" of stratigraphic and geomorphic experiments. Earth Sci. Rev. 97, 1–43.

Perron, J.T., Kirchner, J.W., Dietrich, W.E., 2009. Formation of evenly spaced ridges and valleys. Nature 460, 502–505.

Reiners, P.W., Ehlers, T.A., Mitchell, S.G., Montgomery, D.R., 2003. Coupled spatial variations in precipitation and long-term erosion rates across the Washington cascades. Nature 426, 645–647.

Reinhardt, L., Ellis, M.A., 2015. The emergence of topographic steady state in a perpetually dynamic self-organized critical landscape. Water Resour. Res. 51, 4986–5003.

Riebe, C.S., Kirchner, J.W., Granger, D.E., Finkel, R.C., 2001. Minimal climatic control on erosion rates in the Sierra Nevada, California. Geology 29, 447–450.

Rinaldo, A., Dietrich, W.E., Rigon, R., Vogel, G.K., Rodriguez-Iturbe, I., 1995. Geomorphological signature of varying climate. Nature 374, 632–635.

Rouby, D., Bonnet, S., Guillocheau, F., Gallagher, K., Robin, C., Biancotto, F., Dauteil, O., Braun, J., 2009. Sediment supply to the Orange sedimentary system over the last 150 Myr: an evaluation from sedimentation/denudation balance. Mar. Pet. Geol. 26, 782–794.

Singh, A., Reinhardt, L., Foufoula-Georgiou, E., 2015. Landscape reorganization under changing climatic forcing: results from an experimental landscape. Water Resour. Res. 51, 4320–4337.

Smith, T.R., Bretherton, F.P., 1972. Stability and conservation of mass in drainage basin evolution. Water Resour. Res. 8, 1506–1529.

Stock, J., Dietrich, W.E., 2003. Valley incision by debris flows: evidence for a topographic signature. Water Resour. Res. 39, 1089.

Sweeney, K.E., Roering, J.J., Ellis, C., 2015. Experimental evidence for hillslope control of landscape scale. Science 349, 51–53.

Talling, P.J., Stewart, M.D., Stark, C.P., Gupta, S., Vincent, S.J., 1997. Regular spacing of drainage outlets from linear fault blocks. Basin Res. 9, 275–302.

Thiede, R.C., Bookhagen, B., Arrowsmith, J.R., Sobel, E.R., Strecker, M.R., 2004. Climatic control on rapid exhumation along the Southern Himalayan Front. Earth Planet. Sci. Lett. 222, 791–806.

Tucker, G.E., Slingerland, R., 1997. Drainage basin response to climate change. Water Resour. Res. 33, 2031–2047.

Turowski, J.M., Lague, D., Crave, A., Hovius, N., 2006. Experimental channel response to tectonic uplift. J. Geophys. Res. 111, F03008. https://doi.org/10.1029/2005JF000306.

Von Blanckenburg, F., 2005. The control mechanisms of erosion and weathering at basin scale from cosmogenic nuclides in river sediment. Earth Planet. Sci. Lett. 237, 462–479.

Whipple, K.X., 2001. Fluvial landscape response time: how plausible is steady state denudation? Am. J. Sci. 301, 313–325.

Whipple, K.X., 2009. The influence of climate on the tectonic evolution of mountain belts. Nat. Geosci. 2. https://doi.org/10.1038/ngeo413.

Whipple, K.X., Meade, B.J., 2006. Orogen response to changes in climatic and tectonic forcing. Earth Planet. Sci. Lett. 243, 218–228.

Whipple, K.X., Tucker, G.E., 1999. Dynamics of the stream-power river incision model: implications for height limits of mountain ranges, landscape response timescales, and research needs. J. Geophys. Res. 104, 661–674.

Whipple, K.X., Kirby, E., Brocklehurst, S.H., 1999. Geomorphic limits to climate-induced increases in topographic relief. Nature 401, 39–43.

Willenbring, J.K., Jerolmack, D.J., 2016. The null hypothesis: global steady rates of erosion, weathering fluxes and shelf sediment accumulation during the Late Cenozoic mountain uplift and glaciation. Terra Nova 28, 11–18.

Willett, S.D., 1999. Orogeny and orography: the effects of erosion on the structure of mountain belts. J. Geophys. Res. 104, 28957–28981.

Zachos, J., Pagani, M., Sloan, L., Thomas, E., Billups, K., 2001. Trends, rhythms, and aberrations in global climate 65 Ma to present. Science 292, 686–693.

Zhang, P., Molnar, P., Downs, W.R., 2001. Increased sedimentation rates and grain sizes 2–4 Myr ago due to the influence of climate change on erosion rates. Nature 410, 891–897.